Journal of Quantitative Spectroscopy & Radiative Transfer 133 (2014) 520–525

Contents lists available at ScienceDirect

Journal of Quantitative Spectroscopy & Radiative Transfer

journal homepage: www.elsevier.com/locate/jqsrt

Scattering from a large cylinder with an eccentrically embedded core: An orders-of-scattering approximation

A.J. Yuffa [a,*], P.A. Martin [b], J.A. Scales [a]

[a] Department of Physics, Colorado School of Mines, Golden, CO 80401, USA
[b] Department of Applied Mathematics and Statistics, Colorado School of Mines, Golden, CO 80401, USA

ARTICLE INFO

Article history:
Received 4 June 2013
Received in revised form
12 September 2013
Accepted 14 September 2013
Available online 21 September 2013

Keywords:
Electromagnetic scattering
Lorenz–Mie theory
Orders-of-scattering approximation
Eccentric cylinder

ABSTRACT

We develop an orders-of-scattering approximation, termed the "screened cylindrical void/core" (SCV) approximation, for a composite cylinder. The composite cylinder consists of a large host cylinder that contains a small, eccentrically embedded, core cylinder. The SCV approximation is developed via separation of variables in conjunction with addition theorems for cylindrical functions. We show that the SCV approximation is in good agreement with the numerically exact solution. A simple physical interpretation of the SCV approximation is also presented.

© 2013 Elsevier Ltd. All rights reserved.

1. Introduction

Consider a monochromatic plane wave scattering from an infinitely long isotropic composite cylinder. The composite cylinder is composed of a small core cylinder of radius b that is eccentrically embedded into a large host cylinder of radius a, as shown in Fig. 1. To *experimentally* isolate the core cylinder's contribution to the scattered field of the composite cylinder, one would measure the total field $U^{(1)}$ outside the composite cylinder and the total field $\mathbb{U}^{(1)}$ outside an identical host cylinder. Then, the difference, $V^{(\mathrm{sca})}(r,\theta)=U^{(1)}(r,\theta)-\mathbb{U}^{(1)}(r,\theta)$, would contain the effect that the core cylinder had on the scattered field. In our recent paper [1], we considered the simplest composite cylinder geometry (the core cylinder is *concentric* with the host cylinder) and developed an approximation to $V^{(\mathrm{sca})}$, which we termed the "screened cylindrical void/core" (SCV) approximation. In this paper, we derive an analogous formula for an eccentrically stratified composite cylinder, which can also be interpreted as an orders-of-scattering approximation. Furthermore, we numerically investigate the accuracy of the SCV approximation when $|k_2|a\approx 300$ and $0<|k_3|b\le 1$, where k_2 (k_3) is the wavenumber in the host (core) cylinder.

Scattering by an eccentrically stratified composite cylinder has previously been considered in the literature in various contexts [2–4] and by various techniques [5–7]. In the electromagnetic context, a perturbation series solution has been constructed in powers of (k_3-k_2) [8,9], b [10], and eccentricity [11,12] by using separation of variables. An "exact" treatment based on separation of variables with a truncation of the resultant infinite size matrix is also available, e.g. in [13]. Our orders-of-scattering approach is also based on separation of variables, but the resultant power series expansion of the solution is different from the ones mentioned above.

There are many diverse applications where the scattering by an eccentrically stratified composite cylinder is important, for example, see [4,8,9] and references therein. As mentioned in [1], we are particularly interested in using the composite cylinder to experimentally study Anderson

* Corresponding author. Tel.: +1 720 933 0654.
E-mail addresses: ayuffa@gmail.com (A.J. Yuffa), pamartin@mines.edu (P.A. Martin), jscales@mines.edu (J.A. Scales).

0022-4073/$ - see front matter © 2013 Elsevier Ltd. All rights reserved.
http://dx.doi.org/10.1016/j.jqsrt.2013.09.014

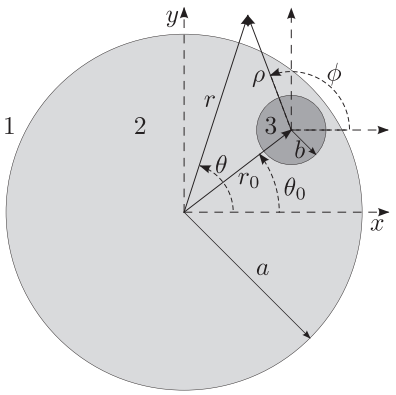

Fig. 1. The cross-sectional view of the composite cylinder, with regions labeled by a number, is shown. Region 1 is the space outside of the composite cylinder ($r>a$), Region 2 is the host cylinder, and Region 3 is the core cylinder. The origin of the (r,θ) coordinate system, where $-\pi\le\theta<\pi$, is centered on the host cylinder, and the origin of the (ρ,ϕ) coordinate system, where $-\pi\le\phi<\pi$, is centered on the core cylinder. The axes of these two coordinate systems are parallel to each other and the center of the (ρ,ϕ) coordinate system is offset by $r_0\cos\theta_0\hat{\mathbf{x}}+r_0\sin\theta_0\hat{\mathbf{y}}$ with respect to the origin of the (r,θ) coordinate system.

localization [14–16] at millimeter/sub-millimeter wavelengths. We are currently fabricating a model of a millimeter-wave random medium from a large cylinder of Teflon (ultra low-loss material) with thousands of small holes drilled in a random pattern. To increase the dielectric contrast between the host cylinder and the holes, we envision filling the holes with quartz or fused silica rods; with this dielectric contrast, the Ioffe–Regel criterion [17, Section 7.4.4] for localization requires roughly two/three scatterers (filled holes) per wavelength. Practically, the host cylinder needs to be rather large ($a\sim10$ cm) in order to accommodate thousands of small holes ($b\sim0.3$ mm), thus the numerical examples considered in this paper are for $k_2a\approx300$ and $0<k_3b\le1$. Furthermore, the experimental role of the host cylinder is simply to hold the rods in place, and so it is beneficial to have a solution in which the effects of the host cylinder and the rods on the scattered field can be distinguished. In other words, the SCV approximation developed in this paper for scattering by a single core cylinder eccentrically embedded into a large host may offer valuable physical insight into understanding the experimental model we described above. Moreover, the approach taken in this paper may be extended via a cluster T-matrix as outlined in [18, Chapter 6] to the full envisioned experiment, where thousands of core cylinders are eccentrically embedded into one large host cylinder.

2. Background and conventions

In this paper, we will assume that all fields are polarized in the positive $\hat{\mathbf{z}}$−direction (out of the page in Fig. 1) and have $\exp(-\mathrm{i}\omega t)$ time dependence, where ω is the angular frequency. The permittivity of the space outside the composite cylinder (Region 1 in Fig. 1) is denoted by $\varepsilon_1\in\mathbb{R}^+$, and the permittivity of the host (core) cylinder is denoted by $\varepsilon_2\in\mathbb{C}^+$ ($\varepsilon_3\in\mathbb{C}^+$), where $\mathbb{R}^+$ denotes the positive real numbers and $\mathbb{C}^+$ denotes the complex numbers with positive real and imaginary parts. Furthermore, the core cylinder, host cylinder, and Region 1 in Fig. 1 are assumed to be non-magnetic. Lastly, we will use the Gaussian unit system for all physical quantities and only consider fields that satisfy the two-dimensional (2D) Helmholtz equation.

The radial solution of the 2D Helmholtz equation is composed of a linear combination of an integer order Bessel function of the first kind and an integer order Hankel function of the first kind, which we denote by $J_m(\xi)$ and $H_m(\xi)$, respectively. The functions $J_m(\xi)$ and $H_m(\xi)$ satisfy the Wronskian relationship [19, Section 9.1]:

$$J_m(\xi)H_m'(\xi)-J_m'(\xi)H_m(\xi)=\frac{2\mathrm{i}}{\pi\xi}, \tag{1a}$$

and the recurrence relation [19, Section 9.2]:

$$\Psi_m'(\xi)=\frac{m}{\xi}\Psi_m(\xi)-\Psi_{m+1}(\xi), \tag{1b}$$

where Ψ denotes J or H, and the prime denotes the derivative with respect to the argument. It is convenient to introduce the shorthand curly bracket notation, $\{\Psi_{m+1}(\xi);\Phi_m(\eta)\}$, by which we mean

$$\{\Psi_{m+1}(\xi);\Phi_m(\eta)\}\equiv\Psi_{m+1}(\xi)\Phi_m(\eta)-\frac{\eta}{\xi}\Psi_m(\xi)\Phi_{m+1}(\eta).$$

For example, if Ψ and Φ satisfy (1b), then

$$\{\Psi_{m+1}(\xi);\Phi_m(\eta)\}=\frac{\eta}{\xi}\Psi_m(\xi)\Phi_m'(\eta)-\Psi_m'(\xi)\Phi_m(\eta) \tag{1c}$$

Lastly, we note the Jacobi–Anger expansion of a plane wave [20, p. 37], namely,

$$\mathrm{e}^{\mathrm{i}\xi\cos\theta}=\sum_m\mathrm{i}^mJ_m(\xi)\mathrm{e}^{\mathrm{i}m\theta}, \tag{2}$$

where $\sum_m$ indicates the summation from $m=-\infty$ to $m=\infty$.

3. Host cylinder

Consider a unit plane wave, $\mathbb{U}^{(\mathrm{inc})}=\exp(\mathrm{i}k_1r\cos\theta)$, incident from Region 1 onto the host cylinder, see Fig. 1 with $b=0$ (i.e., without the core cylinder). Then, after decomposing the total field in Region 1 as $\mathbb{U}^{(1)}=\mathbb{U}^{(\mathrm{inc})}+\mathbb{U}^{(\mathrm{sca})}$, we have [1]

$$\begin{bmatrix}\mathbb{U}^{(\mathrm{sca})}(r,\theta)\\ \mathbb{U}^{(2)}(r,\theta)\end{bmatrix}=\sum_m\mathrm{i}^m\begin{bmatrix}\mathbb{A}_mH_m(k_1r)\\ \mathbb{B}_mJ_m(k_2r)\end{bmatrix}\mathrm{e}^{\mathrm{i}m\theta}, \tag{3}$$

where $k_i=\sqrt{\varepsilon_i}\omega/c$ for $i=1,2$ and c is the speed of light in vacuum. In (3), $\mathbb{U}^{(2)}$ denotes the total field inside the host cylinder, and the expansion coefficients are given by

$$\mathbb{A}_m=-\frac{\{J_{m+1}(k_1a);J_m(k_2a)\}}{\{H_{m+1}(k_1a);J_m(k_2a)\}}, \tag{4a}$$

$$\mathbb{B}_m=\frac{-2\mathrm{i}}{\pi k_1a\{H_{m+1}(k_1a);J_m(k_2a)\}}. \tag{4b}$$

4. Composite cylinder

If the plane wave $\mathbb{U}^{(\mathrm{inc})}$ is incident from Region 1 onto the composite cylinder shown in Fig. 1, then the total fields

in Regions 1, 2, and 3 may be written as

$$U^{(1)}(r,\theta)=\mathbb{U}^{(1)}(r,\theta)+V^{(\mathrm{sca})}(r,\theta), \tag{5a}$$

$$U^{(2)}(r,\theta;\rho,\phi)=\mathbb{U}^{(2)}(r,\theta)+V^{(2)}(r,\theta;\rho,\phi), \tag{5b}$$

and

$$U^{(3)}(\rho,\phi)=\sum_m \mathrm{i}^m D_m J_m(k_3\rho)\mathrm{e}^{\mathrm{i}m\phi}, \tag{5c}$$

respectively, where

$$V^{(\mathrm{sca})}(r,\theta)=\sum_m \mathrm{i}^m A_m H_m(k_1 r)\mathrm{e}^{\mathrm{i}m\theta}, \tag{5d}$$

$$V^{(2)}(r,\theta;\rho,\phi)=\sum_m \mathrm{i}^m (B_m J_m(k_2 r)\mathrm{e}^{\mathrm{i}m\theta}+C_m H_m(k_2\rho)\mathrm{e}^{\mathrm{i}m\phi}), \tag{5e}$$

and $k_3=\sqrt{\varepsilon_3}\omega/c$. In writing (5), we are thinking of the composite cylinder as the host cylinder into which a scatterer (the core cylinder) has been inserted. Also, notice that we required $U^{(3)}(\rho,\phi)$ to be finite at $\rho=0$, and imposed the Sommerfeld radiation (*outgoing* cylindrical wave) condition on $V^{(\mathrm{sca})}(r,\theta)$. To find the unknown expansion coefficients in (5), we require that the electric field and its normal derivative be continuous across the $\rho=b$ and $r=a$ interfaces.

To apply the continuity conditions at the $\rho=b$ interface, we first re-express $U^{(2)}(r,\theta;\rho,\phi)$ solely in terms of the (ρ,ϕ) coordinate system by using Graf's addition theorem [20, Section 2.5]; [19, Section 9.2]. Namely, using

$$J_m(k_2 r)\mathrm{e}^{\mathrm{i}m\theta}=\sum_n J_{m-n}(k_2 r_0)\mathrm{e}^{\mathrm{i}(m-n)\theta_0}J_n(k_2\rho)\mathrm{e}^{\mathrm{i}n\phi},$$

and (3) with (2), we obtain

$$U^{(2)}(\rho,\phi)=\sum_n \mathrm{i}^{-n}J_n(k_2\rho)\mathrm{e}^{\mathrm{i}n\phi}\sum_m T_{nm}(\mathbb{B}_m+B_m)+\sum_m \mathrm{i}^m C_m H_m(k_2\rho)\mathrm{e}^{\mathrm{i}m\phi},$$

where $T_{nm}=\mathrm{i}^{m+n}J_{m-n}(k_2 r_0)\mathrm{e}^{\mathrm{i}(m-n)\theta_0}$. Then, requiring that $U^{(2)}=U^{(3)}$ and $(\partial/\partial\rho)U^{(2)}=(\partial/\partial\rho)U^{(3)}$ on $\rho=b$ yields

$$D_p J_p(k_3 b)=C_p H_p(k_2 b)+(-1)^p J_p(k_2 b)\sum_m T_{pm}(\mathbb{B}_m+B_m), \tag{6a}$$

and

$$\frac{k_3}{k_2}D_p J_p'(k_3 b)=C_p H_p'(k_2 b)+(-1)^p J_p'(k_2 b)\sum_m T_{pm}(\mathbb{B}_m+B_m), \tag{6b}$$

respectively. Eliminating D_p from (6) yields

$$C_p=(-1)^p\Delta_p\sum_m T_{pm}(\mathbb{B}_m+B_m), \tag{7a}$$

where

$$\Delta_p=-\frac{\{J_{p+1}(k_3 b);J_p(k_2 b)\}}{\{J_{p+1}(k_3 b);H_p(k_2 b)\}}. \tag{7b}$$

Similarly, to apply the continuity conditions at the $r=a$ interface, we first re-express $U^{(2)}(r,\theta;\rho,\phi)$ solely in terms of the (r,θ) coordinate system by using Graf's addition theorem for $H_m(k_2\rho)\mathrm{e}^{\mathrm{i}m\phi}$ [20, Section 2.5]; [19, Section 9.2]. Namely, using

$$H_m(k_2\rho)\mathrm{e}^{\mathrm{i}m\phi}=\sum_n (-1)^{m-n}J_{m-n}(k_2 r_0)\mathrm{e}^{\mathrm{i}(m-n)\theta_0}H_n(k_2 r)\mathrm{e}^{\mathrm{i}n\theta}$$

for $r>r_0$, and (3) with (2), we obtain

$$U^{(2)}(r,\theta)=\sum_m \mathrm{i}^m(\mathbb{B}_m+B_m)J_m(k_2 r)\mathrm{e}^{\mathrm{i}m\theta}+\sum_n \mathrm{i}^n H_n(k_2 r)\mathrm{e}^{\mathrm{i}n\theta}\sum_m(-1)^m T_{nm}C_m,$$

for $r_0+b<r<a$. Then, requiring that $U^{(1)}=U^{(2)}$ and $(\partial/\partial r)U^{(1)}=(\partial/\partial r)U^{(2)}$ on $r=a$ yields

$$(\mathbb{B}_p+B_p)J_p(k_2 a)+H_p(k_2 a)\sum_m(-1)^m T_{pm}C_m=J_p(k_1 a)+(\mathbb{A}_p+A_p)H_p(k_1 a), \tag{8a}$$

and

$$(\mathbb{B}_p+B_p)J_p'(k_2 a)+H_p'(k_2 a)\sum_m(-1)^m T_{pm}C_m=\frac{k_1}{k_2}\left[J_p'(k_1 a)+(\mathbb{A}_p+A_p)H_p'(k_1 a)\right], \tag{8b}$$

respectively. To solve (8) for A_p in terms of C_m, we eliminate $(\mathbb{B}_p+B_p)$ from (8), and then use (1a) and (4) to rewrite the result as

$$A_p=\mathbb{B}_p\sum_m(-1)^m T_{pm}C_m. \tag{9}$$

To solve (8) for B_p in terms of A_p, we eliminate C_m from (8), and use (1a) to obtain

$$\frac{2\mathrm{i}}{\pi k_1 a}(\mathbb{B}_p+B_p)=(\mathbb{A}_p+A_p)\{H_{p+1}(k_1 a);H_p(k_2 a)\}+\{J_{p+1}(k_1 a);H_p(k_2 a)\}. \tag{10}$$

To simplify (10) further, we substitute (4) into (10) and note that

$$\{J_{p+1}(k_1 a);H_p(k_2 a)\}\{H_{p+1}(k_1 a);J_p(k_2 a)\}-\{J_{p+1}(k_1 a);J_p(k_2 a)\}\{H_{p+1}(k_1 a);H_p(k_2 a)\}=\left(\frac{2}{\pi k_1 a}\right)^2$$

to obtain

$$B_p=\frac{\pi k_1 a}{2\mathrm{i}}\{H_{p+1}(k_1 a);H_p(k_2 a)\}A_p. \tag{11}$$

Finally, substituting (11) into (7a), and putting the result into (9) yields

$$\sum_n(\delta_{mn}-F_{mn})A_n=G_m, \tag{12a}$$

where

$$F_{mn}=\frac{\pi k_1 a}{2\mathrm{i}}\mathbb{B}_m\left(\sum_p T_{mp}\Delta_p T_{pn}\right)\{H_{n+1}(k_1 a);H_n(k_2 a)\}, \tag{12b}$$

$$G_m=\sum_n \mathbb{B}_m\left(\sum_p T_{mp}\Delta_p T_{pn}\right)\mathbb{B}_n, \tag{12c}$$

and δ_{mn} denotes the Kronecker delta function.

Notice that in (12) the core cylinder parameters, namely k_3 and b, are solely contained in Δ_p, see (7b). Furthermore, from (7b) and the small argument forms of J_p and H_p, we see that if the core cylinder is small, then so is Δ_p. This suggests that (12a) can be solved via the Neumann series (Taylor series expansion, if you will), i.e.,

$$\mathbf{A}=(\mathbf{I}-\mathbf{F})^{-1}\mathbf{G}=\sum_{\ell=0}^{\infty}\mathbf{F}^{\ell}\mathbf{G}, \tag{13}$$

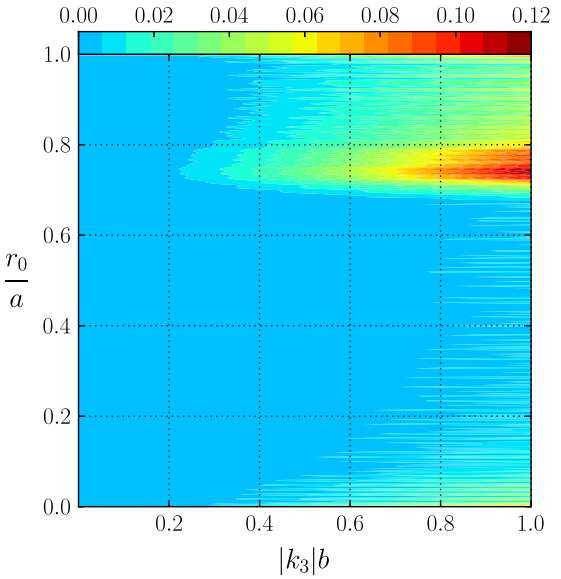

Fig. 2. (color online). The spectral radius of **F** at 100 GHz for a Teflon host cylinder ($a=10$ cm) with an eccentrically embedded quartz core cylinder is shown as a function of $|k_3|b$, and eccentricity, r_0/a (with $\theta_0=0$). The permittivity of Teflon and quartz at 100 GHz is 2.1 and 3.8 with a negligible loss-tangent [22], respectively.

where A_n, F_{mn}, G_m are the elements of **A**, **F**, **G**, respectively, and **I** is the identity matrix. The Neumann series in (13) converges, provided that the spectral radius of **F** is less than one [21, Section 4.3]. The spectral radius of **F** for a large host cylinder, $|k_2|a\approx 300$, with an eccentrically embedded core cylinder is shown in Fig. 2. From Fig. 2, we see that the spectral radius of **F** is indeed much smaller than one and thus, we expect the Neumann series in (13) to converge rapidly. We will discuss the spectral radius of **F** further in Section 6, but for now turn our attention to the physical interpretation of the SCV approximation.

5. The SCV approximation and its physical interpretation

If only the $\ell=0$ term is retained in (13), we obtain the SCV approximation, namely,

$$A_m \cong G_m = \sum_n \mathbb{B}_m \left(\sum_p T_{mp} \Delta_p T_{pn} \right) \mathbb{B}_n. \tag{14}$$

To interpret (14) physically, we consider the following three-step scattering process:

1. If a unit plane wave, $\mathbb{U}^{(\mathrm{inc})} = \exp(\mathrm{i}k_1 r\,\cos\,\theta)$, is incident on the host cylinder, then the field inside the host cylinder, $\mathbb{U}^{(2)}(r,\theta)$, is given by (3). Rewriting $\mathbb{U}^{(2)}$ terms of the (ρ,ϕ) coordinate system yields
$$\mathbb{U}^{(2)}(\rho,\phi) = \sum_n \mathrm{i}^{-n} J_n(k_2\rho)\mathrm{e}^{\mathrm{i}n\phi} \sum_m T_{nm}\mathbb{B}_m. \tag{15}$$

2. If we use (15) as an *incident* field for the core cylinder, then the resulting scattered field is
$$\sum_m \mathrm{i}^m \tilde{C}_m H_m(k_2\rho)\mathrm{e}^{\mathrm{i}m\phi}, \tag{16a}$$
and the field inside the core cylinder is
$$\tilde{U}^{(3)}(\rho,\phi) = \sum_m \mathrm{i}^m \tilde{D}_m J_m(k_3\rho)\mathrm{e}^{\mathrm{i}m\phi}. \tag{16b}$$
Substituting (15) and (16) into the continuity conditions for the $\rho=b$ interface, and eliminating $\tilde{D}_m$ from the resultant two equations, yields
$$\tilde{C}_p = (-1)^p \Delta_p \sum_m T_{pm}\mathbb{B}_m. \tag{17}$$

3. Finally, if we use (16a) with (17) as an *incident* field (from within the host cylinder) on the $r=a$ interface, then there will be an outgoing field outside the host cylinder given by
$$\tilde{V}^{(\mathrm{sca})}(r,\theta) = \sum_m \mathrm{i}^m \tilde{A}_m H_m(k_1 r)\mathrm{e}^{\mathrm{i}m\theta}, \tag{18a}$$
and a regular (finite at $r=0$) field inside the host cylinder given by
$$\sum_m \mathrm{i}^m \tilde{B}_m J_m(k_2 r)\mathrm{e}^{\mathrm{i}m\theta}. \tag{18b}$$
Rewriting (16a) in terms of the (r,θ) coordinate system and substituting it, as well as (18), into the continuity conditions for the $r=a$ interface, and eliminating $\tilde{B}_m$ from the resultant two equations yields
$$\tilde{A}_m = \sum_n \mathbb{B}_m \left(\sum_p T_{mp}\Delta_p T_{pn} \right) \mathbb{B}_n. \tag{19}$$

By comparing (19) with (14), we conclude that the SCV approximation can be viewed as an orders-of-scattering approximation. Moreover, from the above three-step scattering process, we see that $T_{pn}\mathbb{B}_n$ is the "screening" effect of the host cylinder on $\mathbb{U}^{(\mathrm{inc})}$ and $\mathbb{B}_m T_{mp}$ is the "screening" effect of the host cylinder on $\tilde{V}^{(\mathrm{sca})}$. These two screening effects are identical if the core cylinder is *concentric* with the host cylinder, as we have shown in [1]. To see that (19), or equivalently (14), reduces to our previous result, we note that $T_{pn} = \mathrm{i}^{n+p}\delta_{pn}$ and $T_{mp} = \mathrm{i}^{p+m}\delta_{mp}$ when $r_0=0$, and thus, the sums in (19) collapse and we obtain $\tilde{A}_m = \mathbb{B}_m^2 \Delta_m$.

6. Numerical examples and limitations

In practice, the computation of the A_m coefficients via (12) or (14) requires the truncation of the infinite sums, as well as the index m. From (12b), (12c) and (14), we see that the sum over p is controlled by the small core cylinder parameters, namely Δ_p. This observation suggests that the summation over p be terminated at $p_{\max}$ (i.e., $|p|\le p_{\max}$), where $p_{\max}$ is given by the well-known Wiscombe's criterion for small scatterers [23], namely,

$$p_{\max} = \lceil k_2 b + 4(k_2 b)^{1/3} + 1 \rceil. \tag{20a}$$

The sum over n, as well as the index m, is controlled by the large host cylinder and thus, they are terminated at $N_{\max}$ (i.e., $|n|\le N_{\max}$ and $|m|\le N_{\max}$), where $N_{\max}$ is given by the Wiscombe's criterion for relatively large scatterers [23], namely,

$$N_{\max} = \lceil k_1 a + 4.05(k_1 a)^{1/3} + 2 \rceil. \tag{20b}$$

We note that a termination criterion in terms of prescribed relative error has become available recently [24], but for our purposes, the termination condition given by (20) will be sufficient.

To numerically illustrate the accuracy of the SCV approximation, we compute the relative error in the rate at which the energy is extinguished by the core cylinder in the presence of the host cylinder. The rate at which the energy (per unit length of the composite cylinder) is depleted by the core cylinder from the total field, $\mathbb{U}^{(1)}$, outside the host cylinder is given by [1]

$$Q^{\text{ext}} = -\frac{c^2}{2\pi\omega}\sum_{m=-N_{\max}}^{N_{\max}}\left(\text{Re}[A_m] + 2\text{Re}\left[\mathbb{A}_m A_m^*\right]\right), \tag{21}$$

where Re denotes the real part and * denotes the complex conjugate. We compute the SCV approximate and numerically exact (≈ 7 significant digits) Q^{ext} by using (21) with (14) and (21) with (13), respectively. The top row of Fig. 3 shows that the SCV approximation is in good agreement with the numerically exact solution, and the bottom row of Fig. 3 demonstrates that the Neumann series in (13) converges rapidly as one would expect from the spectral radius of $\mathbf{F}$, see Fig. 2. Furthermore, from Fig. 3 we see that the relative error in Q^{ext} is almost independent of the angular position of the core cylinder but does depend on its radial position, see Fig. 3 with $r_0/a > 0.7$.

The dependence of the relative error in Q^{ext} on the radial position of the core cylinder may be explained in terms of the internal resonances of the host cylinder. These resonances are often referred to as Mie resonances, morphological resonances, whispering-gallery modes, or natural/eigenmodes. At 100 GHz, the 10 cm host cylinder is about hundred times larger than the wavelength of the incident light and thus, the interaction of light with the host cylinder can be described by ray theory. If a ray inside the host cylinder strikes the surface of the host cylinder above the critical angle, then the ray's trajectory will be bounded by a cylindrical annulus with outer radius a and inner radius r_{caustic}. To find the caustic radius, r_{caustic}, we set the ray's angular momentum $|k_{2,\theta}|r\hbar$ equal to $|m|\hbar$ (the angular momentum of the mth eigenmode) and note that $k_2^2 = k_{2,\theta}^2 + k_{2,r}^2$ to obtain

$$r_{\text{caustic}} = \left|\frac{m}{k_2}\right|. \tag{22a}$$

In the derivation of (22a), we used the fact that the radial component of the wavevector must vanish on r_{caustic}, i.e., $k_{2,r}(r = r_{\text{caustic}}) = 0$ [25,26]. Furthermore, we can deduce the range of potentially excited eigenmodes of the host cylinder as follows. If a ray inside the host cylinder strikes the surface at an angle γ with respect to the normal, then by equating the ray's and modal angular momenta ($|m| = |k_2|a \sin\gamma$), and using the total internal reflection condition, $\sqrt{\varepsilon_1/\varepsilon_2} \le \sin\gamma \le 1$, we obtain

$$|k_1|a \le m \le |k_2|a. \tag{22b}$$

Finally, from (22), we see why the SCV approximation worsens when the radial location of the core cylinder exceeds the caustic radius, see Fig. 3 for $r_0/a \ge r_{\text{caustic}}/a \approx 0.7$.

If the frequency of the incident wave corresponds to one of the eigenfrequencies of the host cylinder, then the Neumann series in (13) will fail to converge *only* when $r_0 \ge r_{\text{caustic}}$. For example, the mode $m=228$ is excited in resonance at approximately 99.823859 GHz, i.e., the denominator of $\mathbb{B}_{228}$ vanishes at this frequency,[1] and the spectral radius of $\mathbf{F}$ exceeds unity when $r_0/a \le r_{\text{caustic}}/a = 228/(k_2 a) \approx 0.75$ as shown in Fig. 4. Moreover, from Fig. 4 we see that the SCV approximation remains valid even at resonance frequency, provided that $r_0/a < r_{\text{caustic}}/a \approx 0.75$.

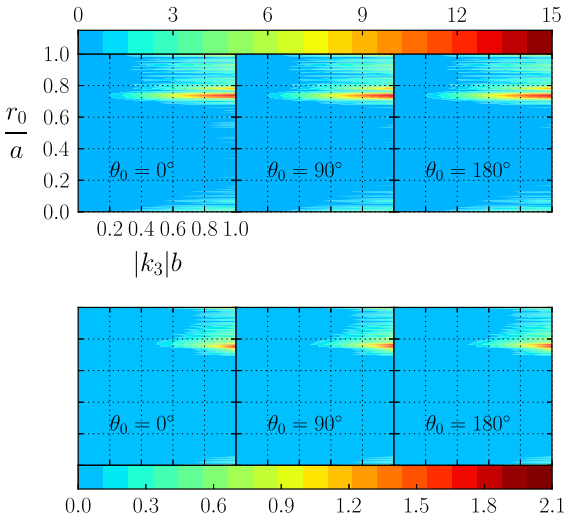

Fig. 3. (color online). The relative error in Q^{ext} (in percent) is shown as a function of $|k_3|b$ and eccentricity, r_0/a, for various θ_0 angles. The top row shows the relative error if only the $\ell = 0$ term is retained in (13), i.e., the SCV approximation, and the bottom row shows the relative error if the $\ell = 0$ and $\ell = 1$ terms are retained. The above plot was produced with the same parameters as the ones described in the caption of Fig. 2.

7. Conclusions

In this paper, we have extended the screen cylindrical void/core (SCV) approximation [1] to a case where the small core cylinder is *eccentrically* embedded into a large host cylinder. We physically interpreted the SCV approximation as the screening effect of the host cylinder on the incident plane wave and the wave scattered by the core cylinder (see Section 5). Furthermore, we showed that the SCV approximation may be thought of as an orders-of-scattering approximation.

The accuracy of the SCV approximation was demonstrated numerically for an envisioned localization experiment, where a large host cylinder ($k_2 a \approx 300$) contains a small ($k_3 b \sim 1$) eccentrically embedded core cylinder. In general, the SCV approximation was shown to be in good agreement with the exact solution, even at the eigenfrequencies of the host cylinder. We showed that if the incident frequency corresponds to one of the eigenfrequencies of the host cylinder, then the SCV approximation remains valid, provided that the eccentricity r_0/a does not exceed the caustic radius of the mode (see Section 6). This

[1] Strictly speaking, this occurs at a *complex* eigenfrequency, where the imaginary part of the eigenfrequency is related to the spectral width of the mode [27].

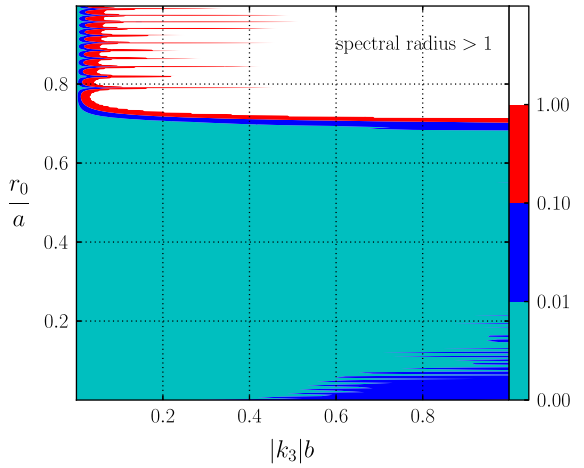

Fig. 4. (color online). The spectral radius of **F** at eigenfrequency 99.823859 GHz is shown as a function $|k_3|b$ and eccentricity, r_0/a (with $\theta_0 = 0$). The above plot was produced with the same parameters as the ones described in the caption of Fig. 2.

condition was derived by considering the interplay between the ray and wave pictures of the scattering process. Moreover, the ray picture offered a valuable physical insight into the validity of the SCV approximation.

Acknowledgments

This material is based upon work supported in part by the U.S. Office of Naval Research as a Multi-disciplinary University Research Initiative on Sound and Electromagnetic Interacting Waves under Grant number N00014-10-1-0958.

References

[1] Yuffa AJ, Scales JA. Measuring the void: Theoretical study of scattering by a cylindrical annulus. J Quant Spectrosc Radiat Transfer (2013). http://dx.doi.org/10.1016/j.jqsrt.2013.02.017.
[2] Roumeliotis JA, Kakogiannos NB. Acoustic scattering from an infinite cylinder of small radius coated by a penetrable one. J Acoust Soc Am 1995;97:2074–81.
[3] Noël J-MA, Patitsas AJ. Modes of vibration in an ideal fluid bounded by two eccentric rigid infinite circular cylindrical boundaries. Can J Phys 1998;76:729–38.
[4] Cai L-W. Scattering of elastic anti-plane shear waves by multilayered eccentric scatterers. Q J Mech Appl Math 2005;58:165–83.
[5] Shaw RP, George T. Time harmonic acoustic radiation from noncon-centric circular cylinders. J Acoust Soc Am 1974;56:1437–43.
[6] Yuan X, Lynch DR, Strohbehn JW. Coupling of finite element and moment methods for electromagnetic scattering from inhomogeneous objects. IEEE Trans Antennas Propag 1990;38:386–93.
[7] Danila EB, Conoir JM, Izbicki JL. Generalized Debye series expansion: part II, treatment of eccentric fluid-solid cylindrical interfaces. Acta Acustica United Acustica 1998;84:38–44.
[8] Uzunoglu NK, Fikioris JG. Scattering from an infinite dielectric cylinder embedded into another. J Phys A Math Gen 1979;12:825–34.
[9] Valagiannopoulos CA. Electromagnetic scattering from two eccentric metamaterial cylinders with frequency-dependent permittivities differing slightly each other. Prog Electromagn Res B 2008;3:23–34.
[10] Roumeliotis JA, Kakogiannos NB. Scattering from an infinite cylinder of small radius embedded into a dielectric one. IEEE Trans Microwave Theory Tech 1994;42:463–70.
[11] Roumeliotis JA, Fikioris JG, Gounaris GP. Electromagnetic scattering from an eccentrically coated infinite metallic cylinder. J Appl Phys 1980;51:4488–93.
[12] Zouros GP, Roumeliotis JA, Stathis G-T. Electromagnetic scattering by an infinite cylinder of material or metamaterial coating eccentrically a dielectric cylinder. J Opt Soc Am A 2011;28:1076–85.
[13] Parrikar RP, Kishk AA, Elsherbeni AZ. Scattering from an impedance cylinder embedded in a nonconcentric dielectric cylinder. IEE Proc H Microwaves Antennas Propag 1991;138:169–75.
[14] Anderson PW. Absence of diffusion in certain random lattices. Phys Rev 1958;109:1492–505.
[15] Lagendijk A, van Tiggelen B, Wiersma DS. Fifty years of Anderson localization. Phys Today 2009;62:24–9.
[16] Sperling T, Bührer W, Aegerter CM, Maret G. Direct determination of the transition to localization of light in three dimensions. Nat Photonics 2013;7:48–52.
[17] Sheng P. Introduction to wave scattering, Localization and mesoscopic phenomena. 2nd ed. Berlin: Springer; 2006.
[18] Yuffa AJ. Modern Electromagnetic scattering. Ph.D. thesis. Colorado School of Mines, 2013.
[19] Abramowitz M, Stegun IA, editors. Handbook of mathematical functions. New York: Dover; 1965.
[20] Martin PA. Multiple scattering. Cambridge: Cambridge University Press; 2006.
[21] Higham NJ. Functions of matrices. Philadelphia: SIAM; 2008.
[22] Goldsmith PF. Quasioptical systems: Gaussian beam quasioptical propagation and applications. New York: Wiley-IEEE Press; 1998.
[23] Wiscombe WJ. Improved Mie scattering algorithms. Appl Opt 1980;19:1505–9.
[24] Neves AAR, Pisignano D. Effect of finite terms on the truncation error of Mie series. Opt Lett 2012;37:2418–20.
[25] Roll G, Schweiger G. Geometrical optics model of Mie resonances. J Opt Soc Am A 2000;17:1301–11.
[26] Schulte J, Schweiger G. Resonant inelastic scattering by use of geometrical optics. J Opt Soc Am A 2003;20:317–24.
[27] Conwel PR, Barber PW, Rushforth CK. Resonant spectra of dielectric spheres. J Opt Soc Am A 1984;1:62–7.